Publication Date: 02 September 2026
Archs Sci. (2026) Volume 75, Issue 6 Pages 1-8, Paper ID 2025601.
https://doi.org/10.68304/as/75601

Warming Contrasts in Tropical Soil Respiration: What Published Model Summaries Can Tell Us

Ashaq Ali, Muhammad Ajmal and Maqbool Ahmad
Department of Mathematics and Statistics, The University of Lahore, Lahore, Pakistan
Corresponding authors: Ashaq Ali (e-mail: arhamusman2001@gmail.com).

Abstract Warming can increase soil respiration while reducing its fitted temperature sensitivity, but these results describe different comparisons. We examine which comparisons can be recovered from the Tropical Responses to Altered Climate Experiment in Puerto Rico. Using fourteen generalized least-squares coefficients, their marginal standard errors, and three annualized efflux increments, we calculate matched-condition treatment ratios, bound uncertainty over admissible coefficient covariances, and assess sensitivity to spatial weights. Shared moisture terms cancel from the treatment contrast. At $24\,^{\circ}\mathrm{C}$, warmed-to-ambient geometric-mean ratios are 1.066, 1.465, and 3.284 for the lower, middle, and upper plot pairs. The warmed-to-ambient Q_{10} ratio is 0.284 (conditional 95% normal-Wald interval: 0.170–0.472). In contrast, an interval for warmed Q_{10} lying wholly below unity requires a correlation below -0.747 between the temperature and treatment–temperature coefficient estimates. Equal weighting of the annualized increments gives 32.63 $\mathrm{Mg\,C\,ha^{-1}\,yr^{-1}}$, with 83.45% contributed by the upper pair; the lower–middle mean is 8.10 $\mathrm{Mg\,C\,ha^{-1}\,yr^{-1}}$. The results establish a lower fitted thermal multiplier and strong concentration of additional efflux among the measured pairs. They do not identify physiological acclimation or a landscape carbon budget. Recovering the missing coefficient covariance and documenting environmental overlap and representative spatial weights would resolve distinct limits on interpretation.

Index Terms soil carbon, thermal sensitivity, generalized least squares, coefficient covariance, spatial weighting, tropical forest

I. Introduction

A warming experiment can produce higher soil respiration and a lower fitted temperature sensitivity at the same time. The two results describe different comparisons: the first concerns efflux under different treatment regimes, whereas the second concerns the temperature slope within a regime. A third quantity, the additional carbon released per unit area and year, also depends on temporal integration and spatial representation. Distinguishing these quantities is essential when chamber measurements are used to assess carbon-cycle feedbacks.

The ecological stakes are substantial. Global records show rising heterotrophic respiration, while tropical forest inventories associate temperature with changes in vegetation carbon [1], [2]. Field heating in Panama demonstrated a strong soil-respiration response in an already warm forest [3]; subsequent measurements linked this response to changes in microbial communities [4]. Evidence from boreal and northern hardwood forests shows that moisture and observation period also affect the measured response [5], [6]. These studies establish the importance of warming effects, but their estimates cannot be compared without considering the environmental conditions and biological processes represented.

The conventional Q_{10} measure compresses a temperature slope into a ten-degree multiplier. Laboratory studies can control moisture and substrate availability to investigate physiological responses [7], whereas field syntheses evaluate respiration under changing environmental conditions [8]. Depth and duration matter as well: whole-soil heating has revealed responses below the surface layer, long experiments have recorded changing feedbacks through time, and repeated inventories have documented subsoil carbon-stock loss [9]–[11]. An increase in total chamber efflux alone cannot distinguish root respiration, decomposition, changes in carbon inputs, or losses from particular soil layers.

Moisture adds a further complication. Carbon persistence depends on soil stabilisation capacity [12], and the moisture response of respiration varies with substrate access, oxygen supply, and gas transport [13], [14]. Throughfall manipulation and drought observations in Puerto Rico show that these controls can change across time scales [15], [16]. At the Tropical Responses to Altered Climate Experiment (TRACE), infrared heating affects both understory vegetation and soil [17]. Root measurements therefore provide information that cannot be inferred from total efflux alone [18]. Microbial models offer plausible explanations for changing temperature responses

ARCHIVES DES SCIENCES
A Multidisciplinary Journal

[19], [20], but a regression coefficient does not identify which mechanism operated in a particular plot.

There is also a statistical obstacle. In a model with a treatment–temperature interaction, the treatment coefficient is the contrast at the temperature origin. Centering temperature improves its interpretation, but the standard error of the centered contrast depends on coefficient covariance [21]. Correct interpretation requires combining the relevant main effects and interactions [22] and checking whether both treatments were observed under the conditions being compared. A coefficient table may be sufficient to calculate a point contrast while remaining insufficient to recover its interval [23].

Here we examine what can be learned from the TRACE coefficient estimates, marginal standard errors, and annualized efflux increments. We address three questions. Which matched-temperature treatment contrasts survive cancellation of the shared moisture terms? How much can their uncertainty vary when coefficient covariances are unreported? How strongly does aggregation of the annualized increments depend on the weight assigned to the upper topographic pair? The analysis uses the response structure without refitting the chamber observations. Its contribution is an explicit account of what those numerical summaries determine and what further information is needed.

II. Materials and methods

A. Inputs and units of analysis

Wood et al. [24] report the TRACE warming experiment in the Luquillo Experimental Forest, Puerto Rico. We use their fourteen generalized least-squares (GLS) coefficients and marginal standard errors, the selected-model specification, and three annualized additional-efflux values.

The experiment comprised three heated and three ambient plots of 12 m^2, arranged in lower, middle, and upper topographic pairs. The site is at approximately 18.32465° N, 65.73058° W, with mean annual temperature of $24\,^\circ\mathrm{C}$ and precipitation of 3500 mm. The reported analysis window runs from 28 September 2016 to 5 September 2017 and includes 57,450 respiration measurements under approximately $4\,^\circ\mathrm{C}$ of soil heating. These numbers describe the field study; the inputs to our calculations are the coefficients, errors, and three efflux summaries.

Table 1: GLS coefficients used in the calculations.

Term	Estimate	Standard error
Intercept	−0.485	0.542
Warmed treatment	3.088	0.732
Temperature	0.092	0.021
Moisture basis 1	−9.595	1.304
Moisture basis 2	−6.070	0.903
Middle position	0.048	0.156
Upper position	0.518	0.138
Warmed × temperature	−0.126	0.026
Warmed × middle	0.318	0.198
Warmed × upper	1.125	0.284
Moisture basis 1 × middle	−6.012	1.804
Moisture basis 1 × upper	6.813	2.665
Moisture basis 2 × middle	2.350	1.293
Moisture basis 2 × upper	8.200	1.748

One permanent chamber collar near the centre of each plot sampled a much smaller footprint than the heated area. Environmental probes were installed at three depths; the fitted temperature and moisture covariates came from 10 cm. Repeated measurements increase temporal resolution, but each topographic position still contains only one heated–ambient pair. They do not provide independent replication of position-specific treatment effects across the forest [25].

The selected model uses daily observations, first-order autoregressive residual dependence, and temperature-dependent, chamber-specific variance. Its reported residual correlation parameter is 0.78. The moisture terms are orthogonal polynomial columns generated by `poly(vwc,2)`, rather than raw moisture and moisture squared. The full coefficient covariance matrix and polynomial attributes are absent from the supplied numerical record. Although the publication identifies an observation archive (DOI 10.15485/2568416), we did not retrieve it. We therefore retain the fitted model as a conditional description and do not reassess its likelihood, residual diagnostics, or observation-level quality control.

B. Treatment contrasts at matched conditions

Let F denote daily mean chamber efflux, w indicate treatment, l denote topographic position, and T and m denote soil temperature and moisture. The selected mean structure can be written as

$$\begin{aligned}\eta_{w,l}(T,m) &= \mathrm{E}[\log F \mid w,l,T,m] \\ &= h_l(m) + bT + w\{a + g_l + dT\}, \end{aligned} \tag{1}$$

where $a = 3.088$, $b = 0.092$, $d = -0.126$, and $g_L = 0$, $g_M = 0.318$, $g_U = 1.125$. The function $h_l(m)$ contains the intercept, position effects, shared moisture basis, and moisture–position interactions. There is no treatment–moisture interaction in the selected model.

Subtracting the ambient prediction from the warmed prediction at the same position, temperature, and moisture gives

$$D_l(T) = a + g_l + dT, \qquad R_l(T) = \exp\{D_l(T)\}. \tag{2}$$

All terms in $h_l(m)$ cancel. Thus, the contrast is available without reconstructing the polynomial normalization. This

cancellation is a property of the model specification; it does not mean that moisture has no biological effect. Comparisons at different moisture values would require the missing basis information.

The exponentiated contrast is a ratio of conditional geometric means. Arithmetic means require retransformation using the residual distribution [26]. Under lognormal errors, for example, their ratio includes a factor determined by the difference in residual variances between treatments. We cannot recover that factor from the coefficient table, so the annualized mass-flux increments are analysed separately.

We evaluate Eq. (2) over 22–26 °C, the intersection of the approximate pooled daily ranges reported for ambient (20–26 °C) and warmed (22–32 °C) plots. This is a candidate comparison range. It does not establish temperature–moisture overlap within each pair. Values at 22, 24, and 26 °C are model evaluations rather than observations at those exact conditions. The equality temperature $T_l^* = -(a+g_l)/d$ is where the fitted ratio equals one; it is not a measured ecological threshold.

C. Uncertainty when coefficient covariance is unavailable

For a linear combination $L = \boldsymbol{c}^{\mathsf{T}}\boldsymbol{\beta}$,

$$\operatorname{Var}(L) = \boldsymbol{c}^{\mathsf{T}}\boldsymbol{\Sigma}\boldsymbol{c}, \tag{3}$$

where $\boldsymbol{\Sigma}$ is the coefficient covariance matrix. Marginal standard errors fix its diagonal, leaving the off-diagonal entries unknown. We consider all symmetric positive-semidefinite completions of that diagonal. Positive semidefiniteness is a constraint on the entire matrix, not simply on individual correlations [27].

Proposition 1. *For fixed marginal standard errors s_j, define $q_j = |c_j|s_j$. Over positive-semidefinite covariance matrices with diagonal s_j^2, the standard error of L has sharp bounds*

$$S_{\min} = \max\left\{0,\ 2\max_j q_j - \sum_j q_j\right\}, \quad S_{\max} = \sum_j q_j. \tag{4}$$

Proof. Represent the covariance matrix as a Gram matrix. Multiplying its component vectors by the contrast coefficients gives vectors of lengths q_j; the standard error is the length of their sum. Alignment attains the triangle-inequality upper bound. If the longest vector exceeds the sum of the others, opposing it with the remaining vectors attains the lower bound. Otherwise, the vectors form a closed polygon and the lower bound is zero. Each construction gives a positive-semidefinite Gram matrix with the required diagonal. Singular matrices may attain the endpoints; positive-definite matrices can approach them. □

For exponentiated contrasts, we report $\exp(L \pm 1.96 S_{\max})$ as a pointwise outer envelope of normal-Wald intervals. The envelope is not the recovered confidence interval of the fitted model, and it assigns no probabilities to covariance completions. Each bound is attainable for its own contrast, but all extrema need not arise from one common matrix. The completion set may also include matrices incompatible with the original design and fitted error parameters. Its breadth measures what remains undetermined by the marginal errors, rather than the plausibility of each completion. All interval statements remain conditional on the fitted model and normal approximation [28].

The lower treatment contrast involves two coefficients; the middle and upper contrasts each involve three. Recovering their fitted intervals therefore requires the relevant treatment–temperature and treatment–position covariances. The residual autoregressive parameter, 0.78, supplies none of these: residual persistence and correlation between coefficient estimates are different quantities. Coefficient covariance also depends on the design matrix and observation weights.

For the thermal slopes, define

$$\begin{aligned} Q_C &= \exp(10b), \\ Q_W &= \exp\{10(b+d)\}, \\ Q_W/Q_C &= \exp(10d). \end{aligned} \tag{5}$$

The ratio depends on one interaction coefficient and has an interval determined by its marginal error. In contrast, uncertainty in Q_W depends on $\rho = \operatorname{Corr}(b, d)$ through

$$S_W(\rho) = \sqrt{s_b^2 + s_d^2 + 2\rho s_b s_d}. \tag{6}$$

We solve for the correlation at which the upper normal-Wald limit of $b + d$ reaches zero. This directly separates evidence of a treatment difference in slope from evidence of a negative warmed slope; comparing separate significance labels would not answer that question [29].

D. Spatial weights, rounding, and computation

The three increments are $e_L = 6.5$, $e_M = 9.7$, and $e_U = 81.7$, expressed in $\mathrm{Mg\,C\,ha^{-1}\,yr^{-1}}$. These units describe carbon mass carried by carbon dioxide. For nonnegative weights summing to one,

$$E(\boldsymbol{w}) = 6.5w_L + 9.7w_M + 81.7w_U, \qquad w_L + w_M + w_U = 1. \tag{7}$$

We examine the full weight simplex and the case $w_L = w_M = (1-u)/2$, $w_U = u$. The latter gives $E(u) = 8.1 + 73.6u$ and upper-position contribution $81.7u/E(u)$. Equating upper and remaining contributions gives the weight at which the upper pair accounts for half the total. The weights are assumptions; no geographic area fractions are estimated.

We assess printed precision separately. If coefficients were rounded to the nearest third decimal, each differs from its printed value by at most 0.0005. At positive temperature, the corresponding maximum deviation in $D_L(T)$ is $0.0005(1 + T)$ and in $D_M(T)$ or $D_U(T)$ is $0.0005(2 + T)$. Equality-temperature bounds combine numerator and denominator endpoints. Rounding each annualized increment to one decimal gives any convex combination a maximum rounding error of 0.05 $\mathrm{Mg\,C\,ha^{-1}\,yr^{-1}}$. These are precision bounds, not sampling intervals.

The accompanying Python script uses NumPy [30] to calculate all table entries and figure coordinates from the two input registers. Checks cover moisture cancellation, thermal-slope identities, spatial thresholds, and 6000 generated positive-semidefinite correlation matrices (2000 per position; seed 20250916). The matrices test the algebraic bounds; they are not simulated field observations or samples from a distribution for the missing covariance. Inputs, numerical outputs, environment versions, and plotting code are supplied together to make the calculations reproducible [31].

III. Results

A. Matched treatment ratios vary with temperature and position

At 24 °C, the matched log contrasts are 0.064, 0.382, and 1.189. The corresponding geometric-mean ratios are 1.066, 1.465, and 3.284 for the lower, middle, and upper pairs (Figure 1; Table 2). All three ratios decline with temperature because they share $d = -0.126$. The upper curve remains highest because the treatment–position differences are constant on the log scale.

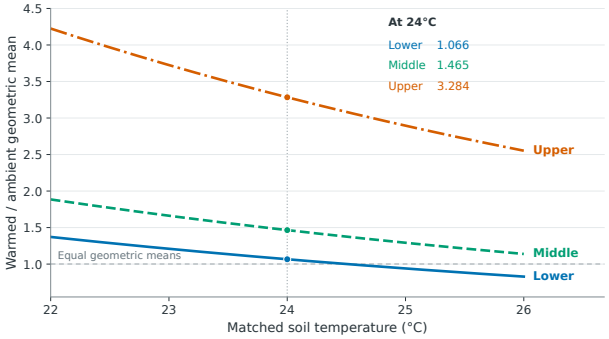

Figure 1: Warmed-to-ambient geometric-mean ratios at matched temperature and moisture. Curves evaluate $R_l(T) = \exp(a + g_l + dT)$ using the GLS coefficients; colours and line styles distinguish the three plot pairs. Points mark 24 °C, with values annotated above the curves. The horizontal reference denotes equal conditional geometric means. The 22–26 °C range is pooled potential overlap, not verified joint environmental support for each pair. Curves are point estimates; covariance-dependent uncertainty at 24 °C is reported in Table 3.

Table 2: Matched ratios and algebraic equality temperatures.

Position	$R(22)$	$R(24)$	$R(26)$	T^* (°C)	Rounding range (°C)
Lower	1.372	1.066	0.829	24.508	24.407–24.610
Middle	1.885	1.465	1.139	27.032	26.917–27.147
Upper	4.225	3.284	2.552	33.437	33.296–33.578

The lower ratio falls from 1.372 at 22 °C to 0.829 at 26 °C. Its fitted crossing, 24.51 °C, lies inside the candidate comparison range. The middle crossing (27.03 °C) lies outside that range, and the upper crossing (33.44 °C) exceeds even the reported warmed range. These are algebraic properties of the fitted lines. None establishes a temperature at which warming would cease to increase respiration in the forest.

A ratio below unity for the lower pair at 26 °C is compatible with its positive annual increment. The matched contrast holds environmental conditions fixed; the annual increment summarizes flux under the conditions experienced by each treatment. Moreover, geometric and arithmetic averaging give different weight to high-flux days. The coefficient table cannot reconstruct their contribution to the integrated carbon mass.

B. Some between-position contrasts retain identifiable intervals

Dividing the upper matched treatment ratio by the lower gives $\exp(1.125) = 3.080$, independent of temperature. The middle-to-lower ratio is $\exp(0.318) = 1.374$. Each uses a single treatment–position coefficient, so its normal-Wald interval follows directly from the reported marginal error: 1.765–5.374 for upper/lower and 0.932–2.026 for middle/lower (Figure 2). These quantities compare treatment ratios, rather than absolute fluxes between positions.

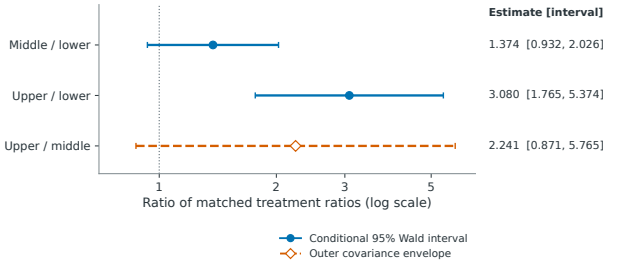

Figure 2: Between-position ratios of matched warming responses. Filled circles and solid lines show estimates and conditional 95% normal-Wald intervals obtained from individual treatment–position coefficients. The open diamond and dashed line show the upper/middle estimate and the outer envelope obtained with the maximum admissible standard error. The latter is not a recovered model confidence interval. Values are printed alongside the logarithmic axis; the vertical reference marks equal warming ratios.

The upper-to-middle estimate is $\exp(1.125 - 0.318) = 2.241$. Its standard error depends on the missing covariance between two interaction coefficients and can range from 0.086 to 0.482. The maximum gives an outer interval envelope of 0.871–5.765. Thus, the available summary specifies the upper/lower interval but does not uniquely determine the upper/middle interval. A significant upper interaction and a nonsignificant middle interaction cannot replace the direct comparison.

C. Covariance uncertainty is much larger than rounding error

For the lower contrast at 24 °C, the marginal-error contributions are 0.732 and $24(0.026) = 0.624$. Their relative alignment permits standard errors from 0.108 to 1.356. Adding the

ARCHIVES DES SCIENCES
A Multidisciplinary Journal

middle or upper interaction widens the attainable ranges to 0–1.554 and 0–1.640, respectively (Table 3). A zero lower endpoint is possible within the mathematical completion set; it does not imply perfect estimation of a field effect.

Table 3: Covariance-completion limits at 24 °C.

Position	Log contrast	Minimum SE	Maximum SE	Outer ratio envelope
Lower	0.064	0.108	1.356	0.075–15.207
Middle	0.382	0.000	1.554	0.070–30.810
Upper	1.189	0.000	1.640	0.132–81.728

The upper ratio of 3.284 has an outer envelope of 0.132–81.728. This wide range describes uncertainty left unresolved by the reporting, rather than an estimated distribution of ecological effect sizes. Setting covariance to zero would select one interval without justification. Centering temperature at 24 °C would improve the treatment coefficient's interpretation but leave its variance dependent on $\mathrm{Var}(a) + 24^2\,\mathrm{Var}(d) + 48\,\mathrm{Cov}(a, d)$.

By comparison, third-decimal rounding changes the matched log contrasts by at most 0.0125 (lower) or 0.0130 (middle and upper), approximately 1.3% on the ratio scale. The equality-temperature ranges in Table 2 span only a few tenths of a degree. More printed digits would therefore improve numerical precision while leaving the main uncertainty problem unresolved.

D. Lower temperature sensitivity does not establish a negative warmed slope

The fitted thermal multipliers are $Q_C = 2.509$ and $Q_W = 0.712$. Their ratio is 0.284, with a conditional normal-Wald interval of 0.170–0.472. This corresponds to a 71.63% reduction in the fitted ten-degree multiplier. The warmed slope itself is $b + d = -0.034$, but its standard error ranges from 0.005 to 0.047 as the missing correlation varies from -1 to 1.

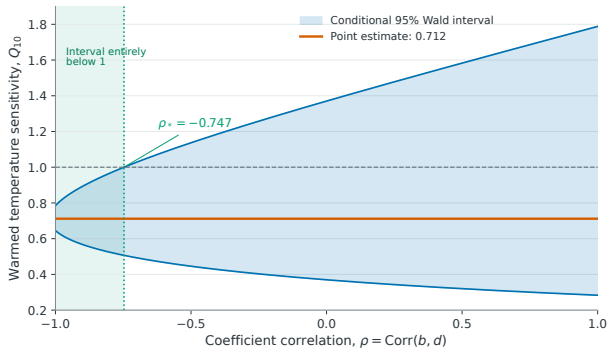

Figure 3: Sensitivity of the warmed Q_{10} interval to unreported coefficient correlation. The blue band gives the conditional 95% normal-Wald interval for $Q_W = \exp\{10(b + d)\}$ as $\rho = \mathrm{Corr}(b, d)$ varies. The point estimate remains 0.712 throughout. The upper interval limit falls below unity only when $\rho < -0.747$ (shaded region). Here ρ concerns estimated regression coefficients, not observed environmental variables. The band displays a sensitivity calculation, not a fitted confidence band over correlation.

At $\rho = 1$, the warmed Q_{10} interval is approximately 0.283–1.788 and includes an increasing temperature response. Its upper limit falls below unity only when $\rho < -0.747$ (Figure 3). The coefficient summary thus gives a directly calculable interval for reduced sensitivity relative to ambient conditions, but a covariance-dependent interval for the sign of the warmed slope.

The ten-degree multiplier is a convention for expressing a fitted slope. The reported ambient range spans about six degrees, and the candidate common range spans four. Consequently, Q_{10} should not be read as a directly observed ten-degree excursion in both treatments.

E. The upper pair dominates the equal-weight increment

The equal-weight mean of the three annualized increments is 32.63 $\mathrm{Mg\,C\,ha^{-1}\,yr^{-1}}$. The upper pair supplies 27.23 $\mathrm{Mg\,C\,ha^{-1}\,yr^{-1}}$ of that mean, or 83.45%; the lower and middle pairs supply 2.17 and 3.23 $\mathrm{Mg\,C\,ha^{-1}\,yr^{-1}}$. Excluding the upper pair and averaging the other two gives 8.10 $\mathrm{Mg\,C\,ha^{-1}\,yr^{-1}}$, 75.18% below the three-pair mean. Both retained increments remain positive. Table 4 collects the increments and derived aggregation quantities.

Table 4: Annualized increments and explicit aggregation quantities.

Quantity	Value
Lower increment ($\mathrm{Mg\,C\,ha^{-1}\,yr^{-1}}$)	6.5
Middle increment ($\mathrm{Mg\,C\,ha^{-1}\,yr^{-1}}$)	9.7
Upper increment ($\mathrm{Mg\,C\,ha^{-1}\,yr^{-1}}$)	81.7
Equal weight across three positions ($\mathrm{Mg\,C\,ha^{-1}\,yr^{-1}}$)	32.63
Equal weight across lower and middle ($\mathrm{Mg\,C\,ha^{-1}\,yr^{-1}}$)	8.10
Upper contribution under three equal weights (%)	83.45
Reduction after excluding the upper pair (%)	75.18
Upper weight giving half the contribution (%)	9.02

Across all nonnegative spatial weights, the aggregate spans 6.5–81.7 $\mathrm{Mg\,C\,ha^{-1}\,yr^{-1}}$ (Figure 4). The lower–middle edge of the simplex covers only 6.5–9.7 $\mathrm{Mg\,C\,ha^{-1}\,yr^{-1}}$, whereas movement towards the upper vertex produces a much larger change. This follows from the contrast between the upper increment and the other two. The triangle represents possible weights, not a geographic map or a continuous model of elevation.

ARCHIVES DES SCIENCES
A Multidisciplinary Journal

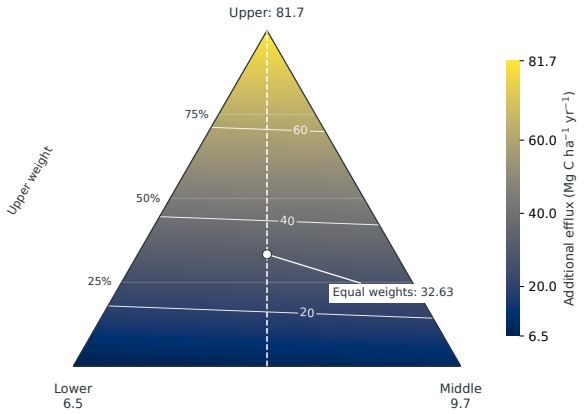

Figure 4: Weighted annualized additional efflux for all allocations among the three positions. Each vertex assigns weight one to its named position; interior points mix the three increments according to Eq. (7). Colours and labelled contours give additional efflux in $\mathrm{Mg\,C\,ha^{-1}\,yr^{-1}}$. Horizontal guides mark the upper-position weight. The white point denotes equal weights and 32.63 $\mathrm{Mg\,C\,ha^{-1}\,yr^{-1}}$; the dashed path has equal lower and middle weights and is examined in Figure 5. No landscape area fractions are inferred.

With equal lower and middle weights, the aggregate follows $E(u) = 8.1 + 73.6u$. The upper contribution exceeds half the total when $u > 0.0902$ and reaches 83.45% at $u = 1/3$ (Figure 5). A small assumed upper fraction can therefore dominate the weighted total. This threshold states the weighting assumption needed for dominance; it does not establish the prevalence of upper-position conditions in the forest.

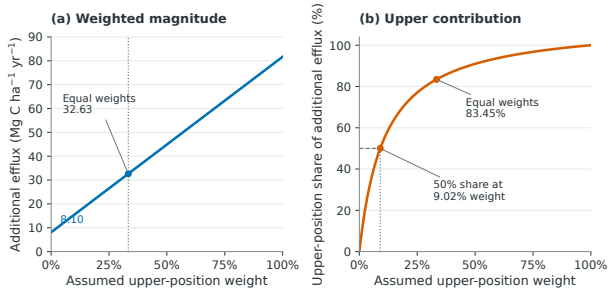

Figure 5: Aggregate magnitude and upper-position contribution along the equal lower–middle weighting path. Both panels use $w_U = u$ and $w_L = w_M = (1-u)/2$. (a) Weighted additional efflux, $E(u) = 8.1 + 73.6u$, with the equal-weight value marked. (b) The upper term's share, $81.7u/E(u)$; it reaches 50% at an assumed upper weight of 9.02% and 83.45% at equal weights. Points mark calculations, not field observations; neither panel includes sampling uncertainty in the increments.

IV. Discussion

A. What the fitted contrasts mean ecologically

The calculations resolve an apparent tension between elevated respiration under warming and reduced fitted temperature sensitivity. A treatment regime can shift the level of a response while changing its slope, and averaging over the conditions experienced by each regime adds another operation. The matched ratios isolate a particular comparison on the fitted response surface. They do not estimate the annual total treatment effect or assign the response to roots, microbes, or a change in substrate supply.

Even a fully documented negative warmed slope would leave its physiological explanation open. The difficulty of interpreting field-derived temperature sensitivity as an intrinsic biological property is well established [32]. Water distribution, oxygen supply, and substrate access can also shape respiration [33]. Companion root and microbial studies help identify plausible mechanisms, but they cannot supply unmeasured respiratory fractions for these six chamber records. Testing acclimation requires measurements designed to separate biological sources and environmental history.

The upper/lower result similarly concerns the measured plot pairs. A conditional interval above unity supports stronger fitted warming separation in the upper pair under the selected model. With only one pair at each position, it cannot distinguish a general topographic response from other differences among those plots. Replication across positions and landscapes is needed before using the contrast as a transferable topographic effect.

B. From chamber efflux to carbon accounting

The annualized increments answer a different question from the geometric-mean ratios. Their spatial average is well defined once weights are specified, but the experiment does not establish representative area fractions. The 83.45% upper contribution is consequently a property of equal weighting. Global soil-respiration analyses explicitly account for environmental representation [34], yet estimates still diverge substantially [35]. The present calculation illustrates one reason: a large local increment can dominate an aggregate whose representative area remains unknown.

Additional soil carbon dioxide release also differs from net ecosystem carbon loss. Partitioned measurements, such as those used in an alpine whole-soil warming experiment, help separate soil- and root-derived contributions [36]. Carbon storage further depends on inputs, transfers, and microbial regulation [37]. The large upper increment warrants attention, but it cannot alone identify the amount or depth of stock depletion, or whether altered plant inputs offset part of the release.

Temporal integration remains a separate requirement. Annualized increments depend on coverage, treatment of missing periods, and episodic flux peaks. We retain the values without independently reconstructing that integration. Nor do we infer ambient annual flux by dividing the increments by reported percentage changes: such an inversion would require matching averaging periods and definitions. Repeated inventories with compatible depths, carbon concentrations, and bulk-density measurements would be needed for a stock-based assessment.

C. Reporting that would enable stronger inference

Three additions would answer different unresolved questions. First, the named coefficient covariance matrix, ideally with the fitted model object, would determine the intervals for matched contrasts and the warmed slope. Second, polynomial attributes and pair-specific temperature–moisture records would permit absolute predictions and checks of environmental overlap. Third, a defined target area, defensible spatial weights, and replicated within-position sampling would support landscape aggregation. None of these additions substitutes for the others.

The accompanying files make the present calculations traceable from inputs to tables and figures, following established reproducibility practices [38]. Machine-readable provenance supports reuse [39], but repeatable computation does not establish ecological representativeness. In particular, tighter model intervals would not create additional treatment replication, and denser temporal measurements would not estimate landscape area fractions.

V. Limitations

This is a secondary analysis of numerical summaries. Without the observations, we cannot assess influential dates, flux screening, missing periods, residual distributions, or the adequacy of the fitted variance and autoregressive structures. Numerical checks verify the calculations, not model fit. Any later predictive assessment would need validation that respects the temporal and spatial dependence of ecological records [40].

The covariance bounds condition on fixed printed marginal errors. They exclude uncertainty in those errors, model selection, and restrictions imposed by the unavailable design matrix. Actual fitted intervals could be much narrower than the outer envelopes, while still remaining conditional on model assumptions. Rounding is examined separately and does not represent uncertainty in annual carbon totals.

Pooled temperature ranges do not establish joint environmental overlap in each pair. Algebraic cancellation at matched moisture also does not identify the causal effect of setting temperature while holding a potentially treatment-affected moisture value fixed. The spatial calculations describe alternative weights for three fixed increments; they do not estimate conditions beyond the observed plots or justify extending a one-year response over subsequent decades.

The publication's later spatial survey, comprising 152 measurements in November 2020, is not contemporaneous replication of the 2016–2017 heating period. The source also gives differing September 2016 operational dates. We retain its stated analytical window without attempting to reconcile the observation calendar. These documentation issues do not change the coefficient algebra, but they prevent independent verification of the complete annual integration.

VI. Conclusion

The TRACE summaries support several precise comparisons. At $24\,^{\circ}\mathrm{C}$, matched geometric-mean warming ratios are 1.066, 1.465, and 3.284 for the lower, middle, and upper pairs. The upper/lower ratio of warming responses is 3.080, and the warmed/ambient Q_{10} ratio is 0.284. Their interpretation depends on the comparison being made: reduced fitted sensitivity is distinct from a negative warmed slope, whose interval requires the missing coefficient covariance.

Aggregation introduces a separate dependence on spatial weights. The upper pair accounts for 83.45% of the equal-weight annualized increment, and omitting it reduces the mean from 32.63 to 8.10 $\mathrm{Mg\,C\,ha^{-1}\,yr^{-1}}$. These findings identify strong concentration among the measured pairs without estimating a landscape carbon budget. Complete covariance reporting, verified environmental overlap, and representative spatial sampling would allow the statistical contrasts to support a broader ecological interpretation.

Author Contributions

All authors contributed equally to the conception, development, and preparation of the manuscript. All authors have read and approved the final version of the manuscript for publication.

Data Availability

All data required to support the findings of this study are included within the manuscript.

Conflicts of Interest

The authors declare that there are no conflicts of interest related to this work.

Funding

This research received no external funding.

Declaration of Generative AI and AI-Assisted Technologies in the Preparation of the Manuscript

Artificial intelligence and computational tools were used to assist with code generation, consistency checking, and technical refinement during the preparation of the manuscript. All AI-assisted and computationally generated content was carefully reviewed and verified by the authors, who take full responsibility for the accuracy, integrity, and final content of the manuscript. Artificial intelligence tools were used to assist with code generation and consistency checking. The author reviewed and verified all AI-assisted content and accepts full responsibility for the final manuscript.

References

[1] Bond-Lamberty, B., Bailey, V. L., Chen, M., Gough, C. M., & Vargas, R. (2018). Globally rising soil heterotrophic respiration over recent decades. *Nature*, *560*(7716), 80–83.

[2] Sullivan, M. J. P., Lewis, S. L., Affum-Baffoe, K., Castilho, C., Costa, F., Sanchez, A. C., Ewango, C. E. N., Hubau, W., Marimon, B., Monteagudo-Mendoza, A., Qie, L., Sonké, B., Martinez, R. V., Baker, T. R., Brienen, R. J. W., Feldpausch, T. R., Galbraith, D., Gloor, M., Malhi, Y., . . . Phillips, O. L. (2020). Long-term thermal sensitivity of Earth's tropical forests. *Science*, *368*(6493), 869–874.

[3] Nottingham, A. T., Meir, P., Velasquez, E., & Turner, B. L. (2020). Soil carbon loss by experimental warming in a tropical forest. *Nature*, *584*, 234–237.

[4] Nottingham, A. T., Scott, J. J., Saltonstall, K., Broders, K., Montero-Sanchez, M., Püspök, J., Bååth, E., & Meir, P. (2022). Microbial diversity declines in warmed tropical soil and respiration rise exceed predictions as communities adapt. *Nature Microbiology*, *7*(10), 1650–1660.

[5] Liang, G., Stefanski, A., Eddy, W. C., Bermudez, R., Montgomery, R. A., Hobbie, S. E., Rich, R. L., & Reich, P. B. (2024). Soil respiration response to decade-long warming modulated by soil moisture in a boreal forest. *Nature Geoscience*, *17*(9), 905–911.

[6] Possinger, A. R., Driscoll, C. T., Green, M. B., Fahey, T. J., Johnson, C. E., Koppers, M. M. K., Martel, L. D., Morse, J. L., Templer, P. H., Uribe, A. M., Wilson, G. F., & Groffman, P. M. (2025). Increasing soil respiration in a northern hardwood forest indicates symptoms of a changing carbon cycle. *Communications Earth & Environment*, *6*, 418.

[7] Bradford, M. A., McCulley, R. L., Crowther, T. W., Oldfield, E. E., Wood, S. A., & Fierer, N. (2019). Cross-biome patterns in soil microbial respiration predictable from evolutionary theory on thermal adaptation. *Nature Ecology & Evolution*, *3*, 223–231.

[8] Carey, J. C., Tang, J., Templer, P. H., Kroeger, K. D., Crowther, T. W., Burton, A. J., Dukes, J. S., Emmett, B., Frey, S. D., Heskel, M. A., Jiang, L., Machmuller, M. B., Mohan, J., Panetta, A. M., Reich, P. B., Reinsch, S., Wang, X., Allison, S. D., Bamminger, C., . . . Tietema, A. (2016). Temperature response of soil respiration largely unaltered with experimental warming. *Proceedings of the National Academy of Sciences of the United States of America*, *113*(48), 13797–13802.

[9] Hicks Pries, C. E., Castanha, C., Porras, R. C., & Torn, M. S. (2017). The whole-soil carbon flux in response to warming. *Science*, *355*(6332), 1420–1423.

[10] Melillo, J. M., Frey, S. D., DeAngelis, K. M., Werner, W. J., Bernard, M. J., Bowles, F. P., Pold, G., Knorr, M. A., & Grandy, A. S. (2017). Long-term pattern and magnitude of soil carbon feedback to the climate system in a warming world. *Science*, *358*(6359), 101–105.

[11] Soong, J. L., Castanha, C., Hicks Pries, C. E., Ofiti, N., Porras, R. C., Riley, W. J., Schmidt, M. W. I., & Torn, M. S. (2021). Five years of whole-soil warming led to loss of subsoil carbon stocks and increased CO_2 efflux. *Science Advances*, *7*(21), eabd1343.

[12] Hartley, I. P., Hill, T. C., Chadburn, S. E., & Hugelius, G. (2021). Temperature effects on carbon storage are controlled by soil stabilisation capacities. *Nature Communications*, *12*, 6713.

[13] Moyano, F. E., Vasilyeva, N., Bouckaert, L., Cook, F., Craine, J., Curiel Yuste, J., Don, A., Epron, D., Formanek, P., Franzluebbers, A., Ilstedt, U., Kätterer, T., Orchard, V., Reichstein, M., Rey, A., Ruamps, L., Subke, J.-A., Thomsen, I. K., & Chenu, C. (2012). The moisture response of soil heterotrophic respiration: Interaction with soil properties. *Biogeosciences*, *9*, 1173–1182.

[14] Moyano, F. E., Manzoni, S., & Chenu, C. (2013). Responses of soil heterotrophic respiration to moisture availability: An exploration of processes and models. *Soil Biology and Biochemistry*, *59*, 72–85.

[15] Wood, T. E., Detto, M., & Silver, W. L. (2013). Sensitivity of soil respiration to variability in soil moisture and temperature in a humid tropical forest. *PLOS ONE*, *8*(12), e80965.

[16] O'Connell, C. S., Ruan, L., & Silver, W. L. (2018). Drought drives rapid shifts in tropical rainforest soil biogeochemistry and greenhouse gas emissions. *Nature Communications*, *9*, 1348.

[17] Kimball, B. A., Alonso-Rodríguez, A. M., Cavaleri, M. A., & Reed, S. C. (2018). Infrared heater system for warming tropical forest understory plants and soils. *Ecology and Evolution*, *8*(4), 1932–1944.

[18] Tunison, R., Wood, T. E., Reed, S. C., & Cavaleri, M. A. (2024). Respiratory acclimation of tropical forest roots in response to in situ experimental warming and hurricane disturbance. *Ecosystems*, *27*, 168–184.

[19] Allison, S. D., Wallenstein, M. D., & Bradford, M. A. (2010). Soil-carbon response to warming dependent on microbial physiology. *Nature Geoscience*, *3*, 336–340.

[20] Wieder, W. R., Bonan, G. B., & Allison, S. D. (2013). Global soil carbon projections are improved by modelling microbial processes. *Nature Climate Change*, *3*, 909–912.

[21] Schielzeth, H. (2010). Simple means to improve the interpretability of regression coefficients. *Methods in Ecology and Evolution*, *1*(2), 103–113.

[22] Brambor, T., Clark, W. R., & Golder, M. (2006). Understanding interaction models: Improving empirical analyses. *Political Analysis*, *14*(1), 63–82.

[23] Hainmueller, J., Mummolo, J., & Xu, Y. (2019). How much should we trust estimates from multiplicative interaction models? Simple tools to improve empirical practice. *Political Analysis*, *27*(2), 163–192.

[24] Wood, T. E., Tucker, C., Alonso-Rodríguez, A. M., Loza, M. I., Grullón-Penkova, I. F., Cavaleri, M. A., O'Connell, C. S., & Reed, S. C. (2025). Warming induces unexpectedly high soil respiration in a wet tropical forest. *Nature Communications*, *16*, 8222.

[25] Hurlbert, S. H. (1984). Pseudoreplication and the design of ecological field experiments. *Ecological Monographs*, *54*(2), 187–211.

[26] Duan, N. (1983). Smearing estimate: A nonparametric retransformation method. *Journal of the American Statistical Association*, *78*(383), 605–610.

[27] Higham, N. J. (2002). Computing the nearest correlation matrix—a problem from finance. *IMA Journal of Numerical Analysis*, *22*(3), 329–343.

[28] Greenland, S., Senn, S. J., Rothman, K. J., Carlin, J. B., Poole, C., Goodman, S. N., & Altman, D. G. (2016). Statistical tests, P values, confidence intervals, and power: A guide to misinterpretations. *European Journal of Epidemiology*, *31*(4), 337–350.

[29] Gelman, A., & Stern, H. (2006). The difference between 'significant' and 'not significant' is not itself statistically significant. *The American Statistician*, *60*(4), 328–331.

[30] Harris, C. R., Millman, K. J., van der Walt, S. J., Gommers, R., Virtanen, P., Cournapeau, D., Wieser, E., Taylor, J., Berg, S., Smith, N. J., Kern, R., Picus, M., Hoyer, S., van Kerkwijk, M. H., Brett, M., Haldane, A., Fernández Del Río, J., Wiebe, M., Peterson, P., . . . Oliphant, T. E. (2020). Array programming with NumPy. *Nature*, *585*(7825), 357–362.

[31] Peng, R. D. (2011). Reproducible research in computational science. *Science*, *334*, 1226–1227.

[32] Subke, J.-A., & Bahn, M. (2010). On the 'temperature sensitivity' of soil respiration: Can we use the immeasurable to predict the unknown? *Soil Biology and Biochemistry*, *42*(9), 1653–1656.

[33] Nissan, A., Alcolombri, U., Peleg, N., Galili, N., Jimenez-Martinez, J., Molnar, P., & Holzner, M. (2023). Global warming accelerates soil heterotrophic respiration. *Nature Communications*, *14*, 3452.

[34] Hursh, A., Ballantyne, A., Cooper, L., Maneta, M., Kimball, J., & Watts, J. (2017). The sensitivity of soil respiration to soil temperature, moisture, and carbon supply at the global scale. *Global Change Biology*, *23*, 2090–2103.

[35] Hashimoto, S., Ito, A., & Nishina, K. (2023). Divergent data-driven estimates of global soil respiration. *Communications Earth & Environment*, *4*, 460.

[36] Chen, Y., Qin, W., Zhang, Q., Wang, X., Feng, J., Han, M., Hou, Y., Zhao, H., Zhang, Z., He, J.-S., Torn, M. S., & Zhu, B. (2024). Whole-soil warming leads to substantial soil carbon emission in an alpine grassland. *Nature Communications*, *15*, 4489.

[37] Schimel, J. P., & Schaeffer, S. M. (2012). Microbial control over carbon cycling in soil. *Frontiers in Microbiology*, *3*, 348.

[38] Sandve, G. K., Nekrutenko, A., Taylor, J., & Hovig, E. (2013). Ten simple rules for reproducible computational research. *PLOS Computational Biology*, *9*(10), e1003285.

[39] Wilkinson, M. D., Dumontier, M., Aalbersberg, I. J., Appleton, G., Axton, M., Baak, A., Blomberg, N., Boiten, J.-W., Bonino da Silva Santos, L., Bourne, P. E., Bouwman, J., Brookes, A. J., Clark, T., Crosas, M., Dillo, I., Dumon, O., Edmunds, S., Evelo, C. T., Finkers, R., . . . Mons, B. (2016). The FAIR Guiding Principles for scientific data management and stewardship. *Scientific Data*, *3*, 160018.

[40] Roberts, D. R., Bahn, V., Ciuti, S., Boyce, M. S., Elith, J., Guillera-Arroita, G., Hauenstein, S., Lahoz-Monfort, J. J., Schröder, B., Thuiller, W., Warton, D. I., Wintle, B. A., Hartig, F., & Dormann, C. F. (2017). Cross-validation strategies for data with temporal, spatial, hierarchical, or phylogenetic structure. *Ecography*, *40*(8), 913–929.